NATIONAL AERONAUTICS AND SPACE ADMINISTRATION

Technical Report 32-1198

Experimental Studies in Magneto-Fluid Dynamics: Pipe Flow Through a Solenoid of Finite Length

T. Maxworthy

JET PROPULSION LABORATORY

CALIFORNIA INSTITUTE OF TECHNOLOGY

PASADENA, CALIFORNIA

December 15, 1967

NATIONAL AERONAUTICS AND SPACE ADMINISTRATION

Technical Report 32-1198

Experimental Studies in Magneto-Fluid Dynamics: Pipe Flow Through a Solenoid of Finite Length

T. Maxworthy

Approved by:

Alan L Kistler

A. L. Kistler, *Manager*
Fluid Physics Section

JET PROPULSION LABORATORY
CALIFORNIA INSTITUTE OF TECHNOLOGY
PASADENA, CALIFORNIA

December 15, 1967

TECHNICAL REPORT 32-1198

Prepared Under Contract No. NAS 7-100
National Aeronautics & Space Administration

PRECEDING PAGE BLANK NOT FILMED.

Contents

Table

Contents (contd)

Figures

Contents (contd)

Figures (contd)

Abstract

A liquid sodium tunnel has been designed and built to study aligned fields, magneto-fluid-dynamic (MFD) flows. Its major features and the nature of the flow in the test section are described. In particular, it is found that an exit disturbance, created as the liquid conductor leaves the region of magnetic field, can propagate into the test section and affect the flow there. However, only under the most adverse conditions, i.e., very high magnetic fields and low flow velocities, does this impair the usefulness of the tunnel as a device for the accurate measurement of MFD flows.

Experimental Studies in Magneto-Fluid Dynamics: Pipe Flow Through a Solenoid of Finite Length[1]

I. Introduction

In the summer of 1961, an ambitious program was begun, aimed at attempting to understand the physical processes underlying the motions created by a conducting fluid as it flowed around an object placed in an aligned magnetic field.[2] Once these processes had been exposed, it was hoped that they would be amenable to some reasonable theoretical treatment which would eventually point the way to general principles applicable in a variety of magneto-fluid-dynamic problems. The completion of this program has yet to be realized, so we confine ourselves in this report and in those which follow, to a description of the facility used in this experimental study, and of the flow created in the test section of the device. This is followed by a discussion of measurements of (1) the drag force on spheres and disks (Refs. 1, 2) and (2) the pressure distribution around a sphere placed in such a flow (Ref. 3).

When the project was initiated, the subject was strewn with hypotheses and predictions that still had to be substantiated by accurate experimental observation. These are described as follows:

(1) The existence of the "precursive wake," a region of vorticity and current density generated by the propagation of disturbances ahead of a body when it is placed in an aligned magnetic field.

(2) The nature of the rearward or conventional wake behind a body.

(3) The changes in separation phenomena.

(4) The existence of magneto-fluid-dynamic boundary layers, the interaction between the magnetic field and a flow field distorted by viscous boundary layer displacement effects or by body interactions.

(5) The changes in drag and lift coefficients due to magnetic interactions.

(6) The properties of magneto-turbulence.

We wished to study these interactions in a logical way and make accurate measurements. As will be seen, some of these questions have been satisfactorily answered, while others are still not well understood.

[1] Subtitled "Description and Flow Characteristics of the JPL Liquid Sodium Tunnel."

[2] At upstream infinity, flow and magnetic field are parallel.

Production of such effects requires that the flowing fluid be a good electrical conductor. Most fluids can either be discarded because of their inaccurately known properties (i.e., plasmas) or because of their weak interaction with a magnetic field under practically realizable conditions (i.e., mercury, ionic solutions). Liquid sodium is the outstanding exception. It is inexpensive, the interactions are substantial, and a large body of technical information exists concerning its properties and methods of control. Extensive work, by nuclear engineers, on the use of liquid sodium as a heat-transfer medium, means that it was not necessary to embark upon an extensive hardware development program. The system was, therefore, designed to take the fullest advantage of this knowledge as embodied in Ref. 4.

It is also desirable, in a report such as this, to show to what extent the original design has fulfilled its expectations. Included are sections devoted to the measurements performed in the tunnel using the simplest of the instrumentation, and the pitot-static pressure probe. From these measurements we can find how the velocity and pressure fields are distorted by the presence of the MFD interaction. By making suitable assumptions, it is also possible to infer the distortions of the applied magnetic field which can later be checked against magnetometer measurements and the validity of the assumptions verified. An Appendix on pressure distribution measurements around a sphere placed at various axial locations is included to show how the tunnel is suited to the measurement of aerodynamic flows.

II. Fluid Dynamical Design Parameters

With the addition of two extra quantities to the equations of fluid motion, viz., an electrical conductivity and a magnetic field, we now have three independent nondimensional parameters available to characterize the system. Six possible parameters are shown in Table 1, together with their physical interpretation and typical values for sodium and mercury. Rationalized M.K.S.Q. (meters, kilograms, seconds, charge) units are used throughout. It is quite apparent that sodium is superior in all respects to mercury as a working fluid, unless a mercury system can be made to give accurate answers at very low velocities ($\sim$ 0.01 m/s) and very high magnetic fields (1.2 Wb/m^2). In this table, d and U_∞ are the body dimension and fluid velocity, and ρ, ν, σ and μ are the fluid density, kinematic viscosity, electrical conductivity and permeability; B_∞ is the applied magnetic flux density.

III. Design and Description of the Flow System

Two major criteria must be satisfied by our system: the first requires that we have a vorticity-free, current-free flow of known steady temperature and velocity in the test section; the second requires that the sodium system be as safe as possible. Special handling problems must be solved

Table 1. Characteristic parameters[a]

Parameter	Sodium at 150°C	Mercury
Interaction parameter $N = \frac{B_\infty^2\, d\, \sigma}{\rho\, U_\infty} = \frac{\text{magnetic force}}{\text{inertia force}} = \alpha^2\, Rm = \frac{Ha^2}{Re}$	$0 - 10^2$	$0 - 0.75 \rightarrow 10^2$ for $B = 1.2$ Wb/m^2; $U = 0.01$ m/s
Reynolds number $Re = \frac{U_\infty d}{\nu} = \frac{\text{convected energy}}{\text{viscous dissipation}}$ or $\frac{\text{inertia forces}}{\text{viscous forces}}$	$1 \times 10^4 - 3 \times 10^5$	$4 \times 10^4 - 13 \times 10^5$
Magnetic Reynolds number $Rm = U_\infty d\, \mu\sigma = \frac{\text{convected energy}}{\text{Joule dissipation}}$	0.06 — 1.9	0.006 — 0.19
Alfvén number $\alpha^2 = \frac{B_\infty^2}{U_\infty^2 \rho\mu} = \frac{\text{magnetic energy}}{\text{kinetic energy of directed motion}}$	$0 - 1.7 \times 10^3$	$0 - 1.7 \times 10^2$
Hartman number $Ha = \left(\frac{B_\infty^2\, d^2\sigma}{\rho\nu}\right)^{1/2} = \left(\frac{\text{magnetic force}}{\text{viscous force}}\right)^{1/2}$	$0 - 10^6$	$0 - 3 \times 10^4$
Magnetic Prandtl number $Pr_m = \mu\sigma\nu = \frac{\text{viscous dissipation}}{\text{Joule dissipation}}$ or $\frac{\text{viscous diffusion length}}{\text{magnetic diffusion length}}$	6×10^{-5}	1.5×10^{-7}

[a] Numerical values with $d = 0.01$ m; $U_{max} = 15$ m/s; $U_{min} = 0.5$ m/s; $B_{max} = 0.7$ Wb/m^2; except where noted.

since the fluid must not come into contact with water, oxygen, and many organic substances. Certain fundamental rules should be obeyed,[3] but because of the low operating temperatures of the present system (150°C), optimum component design is not absolutely necessary. For example, breakable joints can use silicone rubber *O*-rings, which would be quite unsuitable at higher temperatures. To satisfy all these conditions, the following flow system (Figs. 1 and 2) was devised with two subsidiary but very necessary systems: a heating circuit to raise and maintain the temperature of the sodium at 150°C, and a dry nitrogen system with which to blanket the sodium to prevent contact with air and manipulate the fluid levels within the tunnel.

During its motion, the fluid passes through the following components: a "free-surface" centrifugal pump, an electromagnetic flowmeter, a wide-angle diffuser and settling chamber, a nozzle, the test section, a narrow-angle diffuser, and a gas trap, finally returning to the pump section. With pump speed control, the fluid flow rate can be varied from 5 to 350 gal/min. By a suitable arrangement of valves, the fluid can be filtered and, by manipulating pressures in the sump tank, in the expansion tank, at the pump discharge, and at the pump-free surface, the system can be filled, pressurized to prevent cavitation in the test section, and emptied when maintenance is necessary. Emergency controls are incorporated so that the total sodium content can be dumped into the sump tank in case leakage occurs in any part of the system.

A magnetic field (produced by a current-carrying solenoid) fills the test section, into which various instrumented probes and body shapes can also be introduced.

The majority of the system requires no further description; however, there are three points which do require further elaboration since they are outside conventional engineering experience.

A. Magnet and Nozzle Design

The form of the magnetic field to be used in our studies has great effect on many of the features of the flow system. It is discussed first so that these features may be logically explained.

We wish, at first, to consider aligned magnetic fields and choose a solenoidal configuration to achieve this end. However, one main difficulty arises with the combination of a stationary field and a flowing conducting fluid. This is explained by reference to Fig. 3(a) where, qualitatively, the interaction between a solenoidal field and a parallel flow field is shown. Interaction between field and flow creates azimuthal currents and vorticity, i.e., distorts both the applied magnetic and velocity fields, which are convected into the test section, destroying our desire for a current-free, vorticity-free flow. To improve the entry effects, several possibilities are available. The one chosen is shown diagrammatically in Fig. 3(b). The convergent nozzle is designed to follow a chosen magnetic streamline over an arbitrarily chosen distance. Because of the identical nature of the equations governing the electromagnetic field and the flow field (neglecting viscosity), the two fields are more closely parallel than before, and reducing the current and vorticity production results in a more uniform test section velocity profile. Unfortunately, the interaction produced at the exit of the test section cannot easily be removed in the same way, and it is this effect which creates the majority of the difficulty in the test section as discussed in Section V.

B. Wide-Angle Diffuser

In order to satisfy the conditions imposed by severe space limitations, it is necessary to decrease the velocity of the flow approaching the test section very rapidly. Using the approach of Schubauer and Spangenburg (Ref. 5), a wide-angle diffuser is filled with screens of appropriate resistance and distribution to effectively prevent separation by changing the pressure distribution within the diffuser. Values were calculated by assuming that the net pressure change in the diffuser is zero, i.e., by putting enough screens in to exactly destroy the pressure increase that occurs due to the increase in area. Initial tests, using water as a fluid, showed that separation was prevented and that a uniform velocity profile existed at the diffuser exit.

C. Test Section, Probe, and Model Traverse

The test section joins continuously to the nozzle and is 2 in. in diameter and 18 in. long. The solenoid surrounding the test section was 15 in. long, producing an axial magnetic field uniform to 3% over the middle 10½ in. A mechanism was built to traverse instrumentation probes within the test section. Complication is added by the need to prevent any leakage of the liquid sodium within the system; hence, bellows seals or free-surface seals are used at all sliding joints. Accurate positioning of all probes is possible to within 0.001 in. in the radial direction and 0.01 in. in the longitudinal direction.

[3] As outlined in Ref. 4.

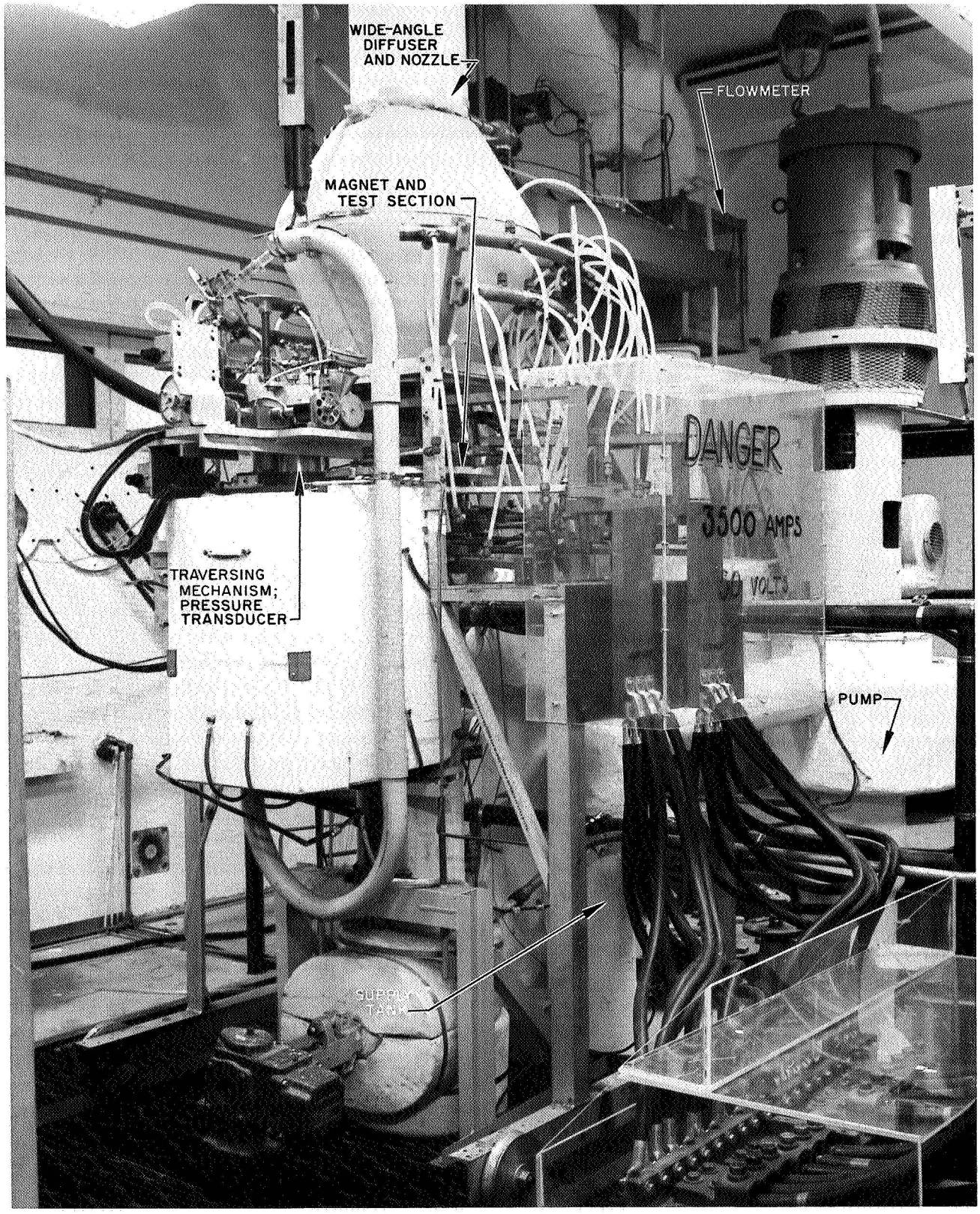

Fig. 1. Photograph of the liquid sodium tunnel, with test section and traversing mechanism in the foreground

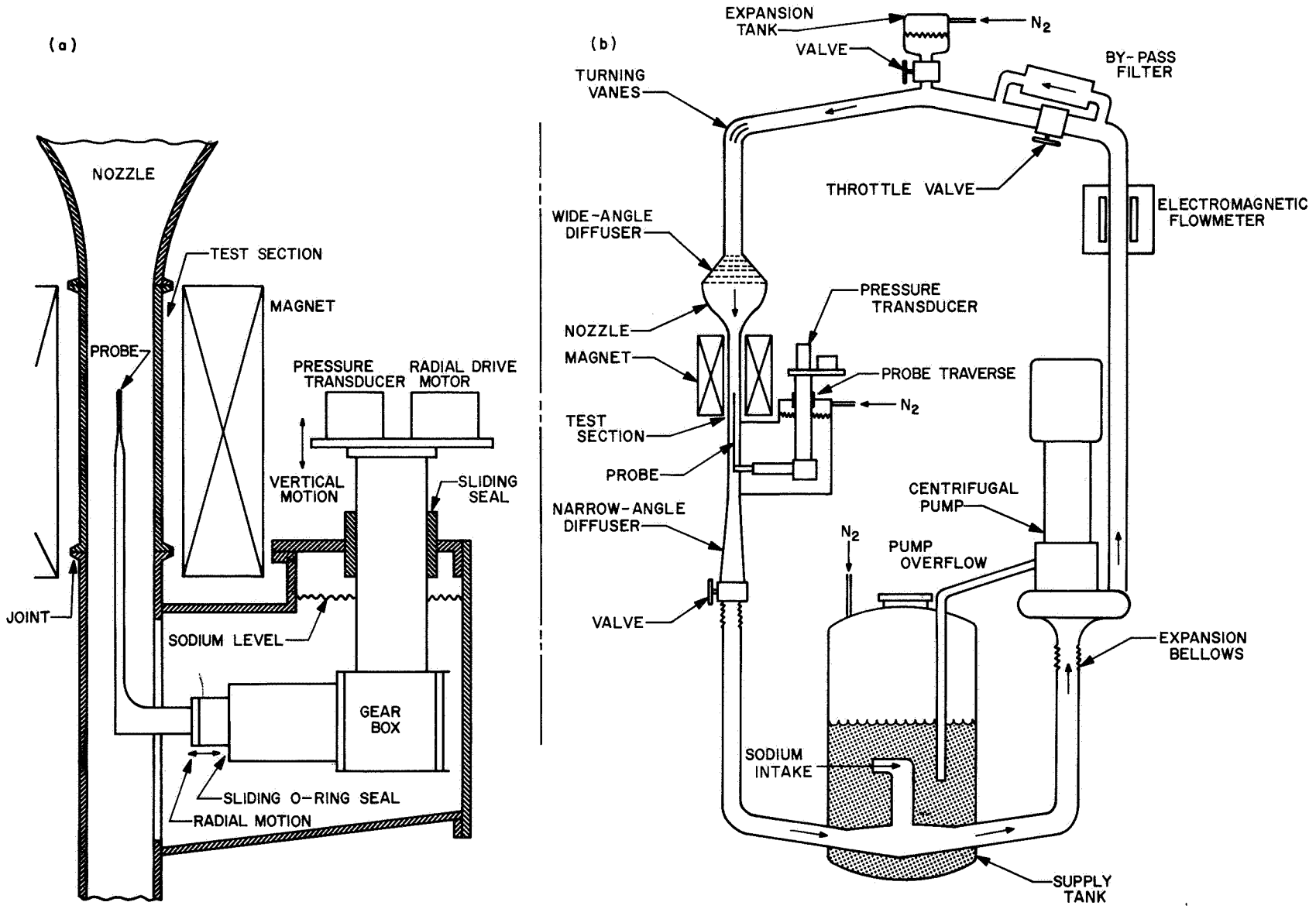

Fig. 2. (a) Diagrammatic view of the liquid sodium flow loop; (b) cross-section through the test section and probe traversing mechanism

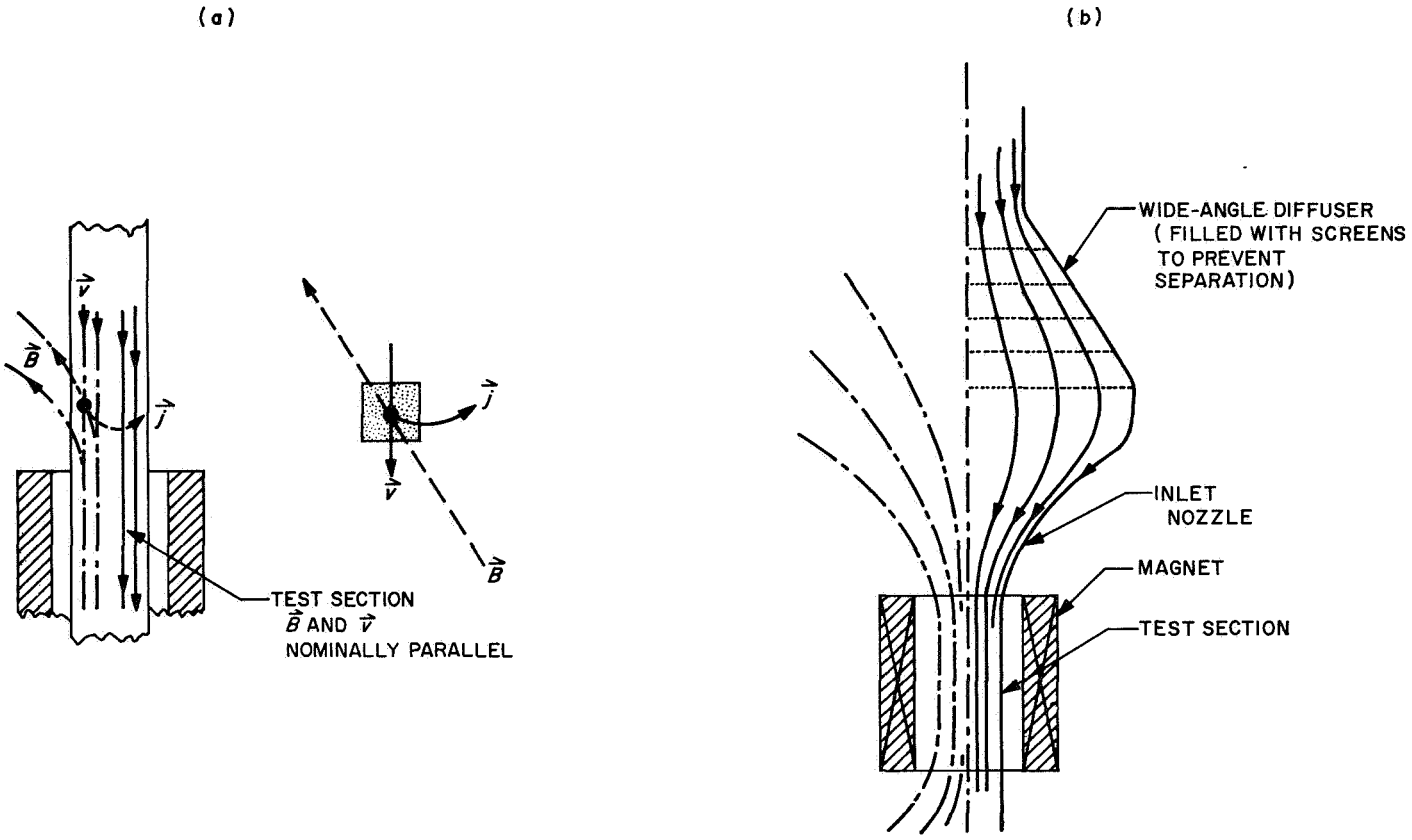

Fig. 3. (a) Interaction between the magnetic field of a solenoid and the flow of an initially parallel stream of conducting fluid; (b) view showing how the interaction between fluid and magnetic field can be modified by shaping of the inlet nozzle

IV. Instrumentation

Instrumentation can be subdivided into devices to measure locally (1) the dependent quantities: pressure, velocity, and magnetic field; and (2) the independent quantities: flow rate, and applied magnetic field.

A. Pressure-Measuring Devices

A conventional pitot-static probe can be used to measure total (P^0), static (P), and dynamic pressure (Q) within the system.

The interaction between the flowing fluid and the applied field creates an electrical current distribution which interacts with the magnetic field to produce a force (Lorentz force) which alters the velocity field. The probe itself creates an interaction which can change the readings that would exist if the probe caused no disturbance. Thus, the probe is in a region in which pressure and Lorentz forces are acting, and without careful thought it is not immediately obvious what such a probe will measure. Consider the force balance on a volume which is constructed just outside the pressure measuring region (Fig. 4). We draw the static pressure hole for convenience, but a similar argument also applies to the total pressure hole. It is assumed that the velocity normal to the measuring plane is insignificant, although if a flow does exist, one only requires a pressure gradient to balance the decelerating force of the flow in order to regain a simple explanation. The only forces acting on the particle are a Lorentz body force and normal surface-pressure forces, assuming viscous forces are negligible. If the particle is in equilibrium, the forces must balance, i.e., Lorentz force equals the difference of the normal pressure forces, or differentially, the Lorentz force equals the pressure gradient. In the region with no Lorentz forces, i.e, $j_0 \equiv 0$, the pressure gradient is zero or the pressure is constant. A combination of these circumstances operates in our case. For the particle just outside the static hole, the Lorentz force is balanced by the pressure gradient so that only the fluid-dynamic pressure force itself acts on the static hole interface. A particle just in the nonconducting fluid, which is

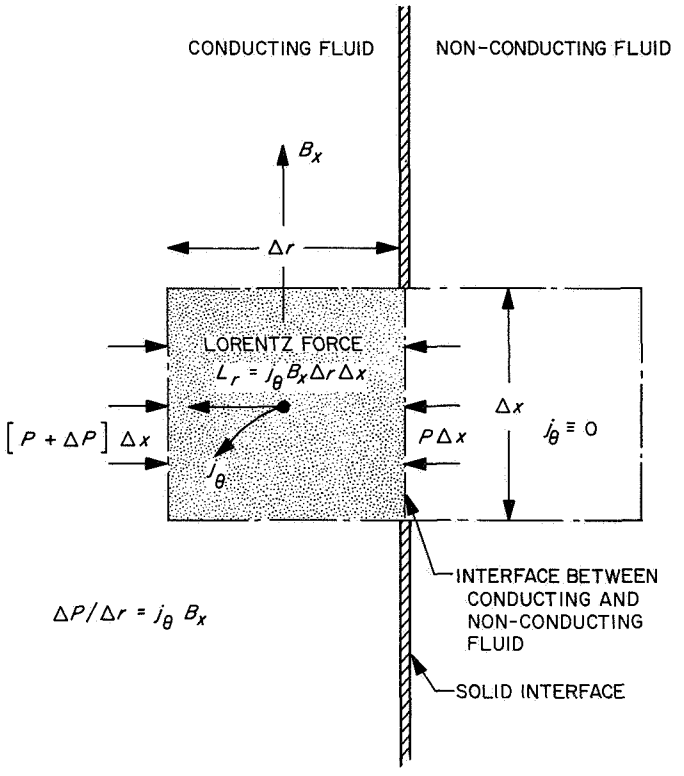

Fig. 4. Diagrammatic view of force balance on particles close to a pressure measuring orifice

used to transmit the pressure to the pressure transducer, has no Lorentz force acting upon it. Therefore, there is no pressure gradient, and the pressure is constant throughout this region and equal to the pressure just outside the static hole. As a result of this seemingly unnecessary explanation, it is believed that the pressures measured by the "static and total pressure" orifices are, in fact, the *local* static and total pressures. These pressures are transmitted to a "Pace" variable reluctance gauge by lines filled with an inert silicone oil of low viscosity. A sensitive ac Wheatstone bridge circuit is used to convert the gauge diaphragm movement to a readable electrical output. The system was calibrated against an accurate mercury manometer over the complete pressure range.

If the total pressure and static pressures are subtracted, then the resultant dynamic pressure, ($\frac{1}{2}\ \rho U^2$), measures the velocity directly. This assumes that the static pressure does not change between the two orifice locations, either due to gradients in the basic flow or to the effect of the probe on the pressure distribution. The former has, in fact, caused considerable difficulty in the interpretation of velocity profiles in the tunnel. Due to the rapid changes in velocity created by an exit MFD interaction, axial and radial static-pressure gradients exist in the lower part of the test section. Since the total and static pressure holes are 1½ in. apart, a static pressure difference can exist between them and can cause the difficulty previously mentioned. Possibly, direct probe interactions also interfere with the accurate measurement of the static pressure; only indirect evidence can be quoted on this point, but for the low values of probe interaction parameter[4] used here such effects are small (see Section IV-C).

B. Magnetic Field

If suitable assumptions are made, it is possible to infer magnetic field distributions from measured static pressure variations within the flow. This is particularly true of radial variations since we need to assume that of all the forces acting on a fluid particle, only the Lorentz force and the pressure gradient force are of great importance since radial particle acceleration is small. For the axial gradients, this is no longer true since acceleration terms may well be comparable to all of the others. Writing the radial momentum equation, using these assumptions, we obtain:

$$-\frac{\partial p}{\partial r} = -j_\theta B_x \approx \frac{1}{\mu}\frac{\partial B_x}{\partial r} B_x = \frac{1}{2\mu}\frac{\partial}{\partial r}(B_x^2) \qquad (1)$$

where we have ignored $\partial B_r/\partial x$ in substituting for j_θ.

Hence

$$\frac{\partial}{\partial r}\left(P + \frac{B_x^2}{2\mu}\right) = 0 \qquad (2)$$

or

$$P + \frac{B_x^2}{2\mu} = \text{constant across the tunnel} \qquad (3)$$

where **B** is the magnetic field, μ is the magnetic permeability, and x, r, and θ are the cylindrical coordinates defining the flow. As discussed, the static pressure probe measures the fluid pressure P, only. Thus, when $B_\infty = 0$, P should be constant; this is well substantiated by measurements in the tunnel. With the magnetic field applied, radial pressure gradients are measured and these infer magnetic field gradient also, which can be calculated.

This scheme has several drawbacks. It can really only measure relative field changes across the tunnel, but by making suitable assumptions, it is possible to infer axial variations. We can make several approximate calculations.

[4] Interaction parameter based on probe diameter.

From $\partial B_x/\partial r$, we can find the current flow at each section since

$$j_\theta \approx \mu \frac{\partial B_x}{\partial r} \tag{4}$$

If this procedure is repeated at various axial stations, we can obtain a complete mapping of the current distribution in the test section. Once the current distribution is known, it is possible, in theory at least, to calculate the complete distribution of **B**. However, this calculation is very tedious since solutions exist only for very simple current distributions, e.g., finite length solenoids, etc.; and the more elaborate ones require extensive machine calculations. In order to gain some simple information from the measured distributions, further and more drastic assumptions have to be made. The real current distribution could be replaced by a distribution of finite length and infinitely thin solenoids with appropriate current distributions. Available calculations could then be used to gain approximate knowledge of the magnetic-field distribution axially. An even more drastic simplification can be used in order to make use of the pressure distributions without major calculation. This makes use of the special character of axisymmetric flow. A change in the magnitude of the central field requires a much smaller change in the magnetic field at the wall in order to satisfy continuity of field, since the central stream tubes only carry a very small fraction of the total magnetic flux through the magnet. To the first order, we assume that the magnetic field at the tube wall is unchanged at the applied value. We can then integrate inwards to find the axial distribution of field on the axis. A second-order correction can be performed in order to see how good our original assumption was. Calculations for several cases show errors on the order of 0.5% in the calculation of the centerline magnetic-field distribution, using these drastic assumptions.

C. Flow Rate

The overall flow rate was monitored by a cross-field electromagnetic flowmeter. This was calibrated by integrating the measured flow velocity in the test section at various nominal flow-meter settings. By integrating velocity profiles with an applied magnetic field in the test section and at these same nominal flow-meter settings, it was possible to infer probe interaction effects. Fortunately, at the small probe interaction parameters encountered, the total flow rates with and without a strong magnetic field were identical, to within experimental error, implying that the velocities measured with and without field were unaffected by probe effects.

D. Applied Magnetic Field

The overall applied magnetic field was monitored in two ways: first, by measuring the output voltage of the power supply, and secondly, by measuring the magnetic field directly using an air-cooled "Hall probe," in the test section itself, coupled to a Bell magnetometer readout.

V. Results and Discussion

The results of such measurements immediately show that the device is not an optimum one for looking at MFD pipe flow. Many small effects oppose and reinforce one another and obscure any simple parametric dependence that might exist in an experiment specifically designed to expose such a dependence. MFD phenomena can be found, however, and at least a qualitative description can be given of their behavior over the operating range of the device. It is found that the highest values of N give the most unambiguous MFD effects, for at low N they are mixed in with the normal behavior of pipe flow with growing boundary layers on the walls, etc., and no purely MFD behavior is easily extracted. Therefore, we finally consider in detail the flow with an applied magnetic field of 0.702 Wb/m^2 and flow rates varying over a factor of 5 from nominally 50–250 gal/min (i.e., velocities from 2 to 10 m/s), and attempt to make some quantitative comments about MFD phenomena that may be of use in understanding other physical situations. Results at smaller values of the applied field show less dramatic deviations from uniform flow and the usefulness of the apparatus is not in doubt.

A. Results and Deductions from Measurements of Static Pressure

Figures 5 and 6 show the most important results of this study. Radial and axial static pressure gradients exist in the flow; they are small at the center of the test section but grow exponentially towards the exit (the region in which the flow is leaving the test section but is still moving through a uniform, applied magnetic field). Certain critical observations can be made from these results. The axial momentum equation can be written:

$$-\frac{\partial P}{\partial x} = \rho j_\theta B_r + \rho v_x \frac{\partial v_x}{\partial x} + \nu \frac{\partial^2 v_x}{\partial r^2} + \text{smaller terms} \tag{5}$$

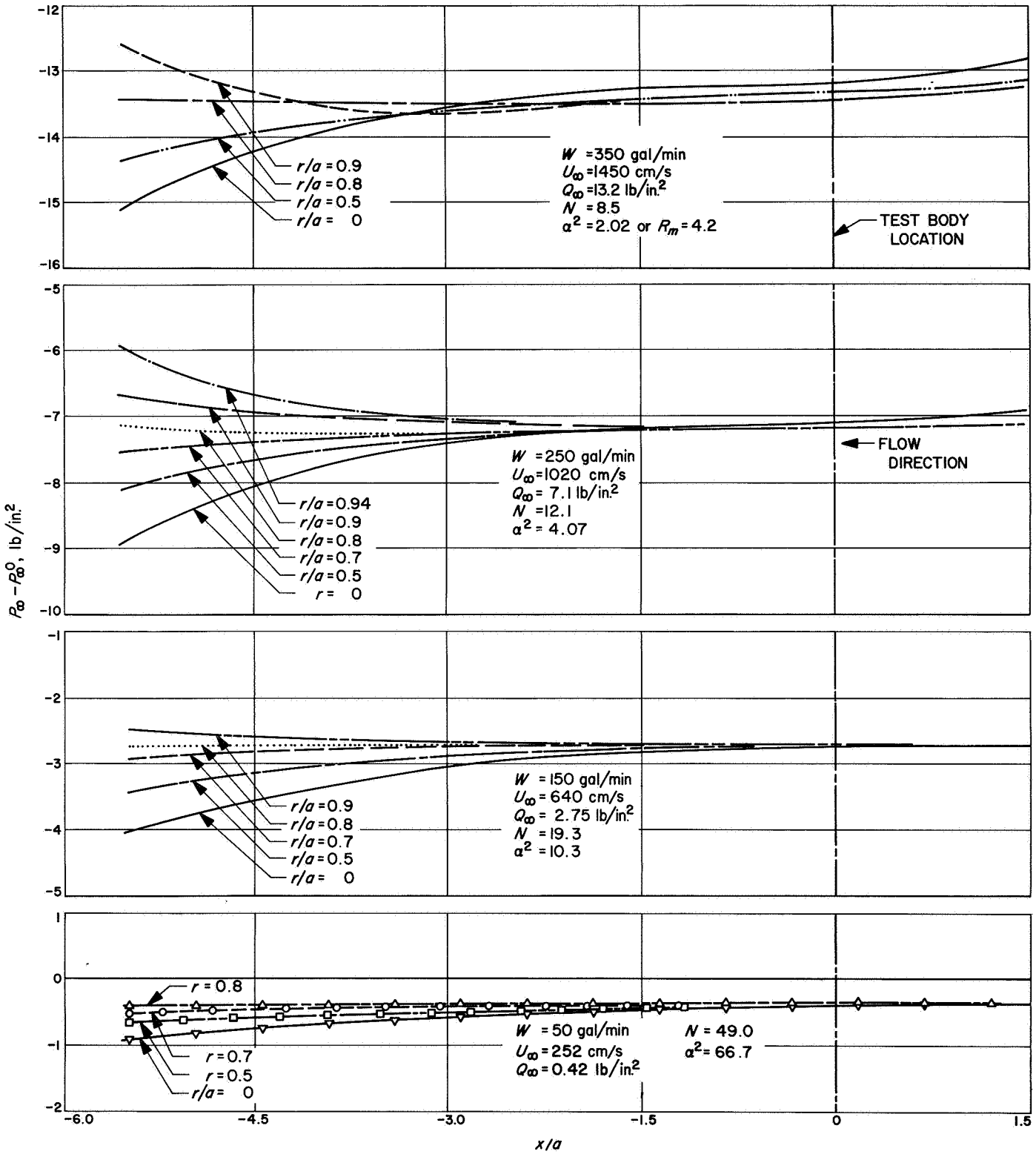

Fig. 5. Longitudinal static pressure profiles at various radial locations and flow rates ($B_\infty = 0.70$ Wb/m²)

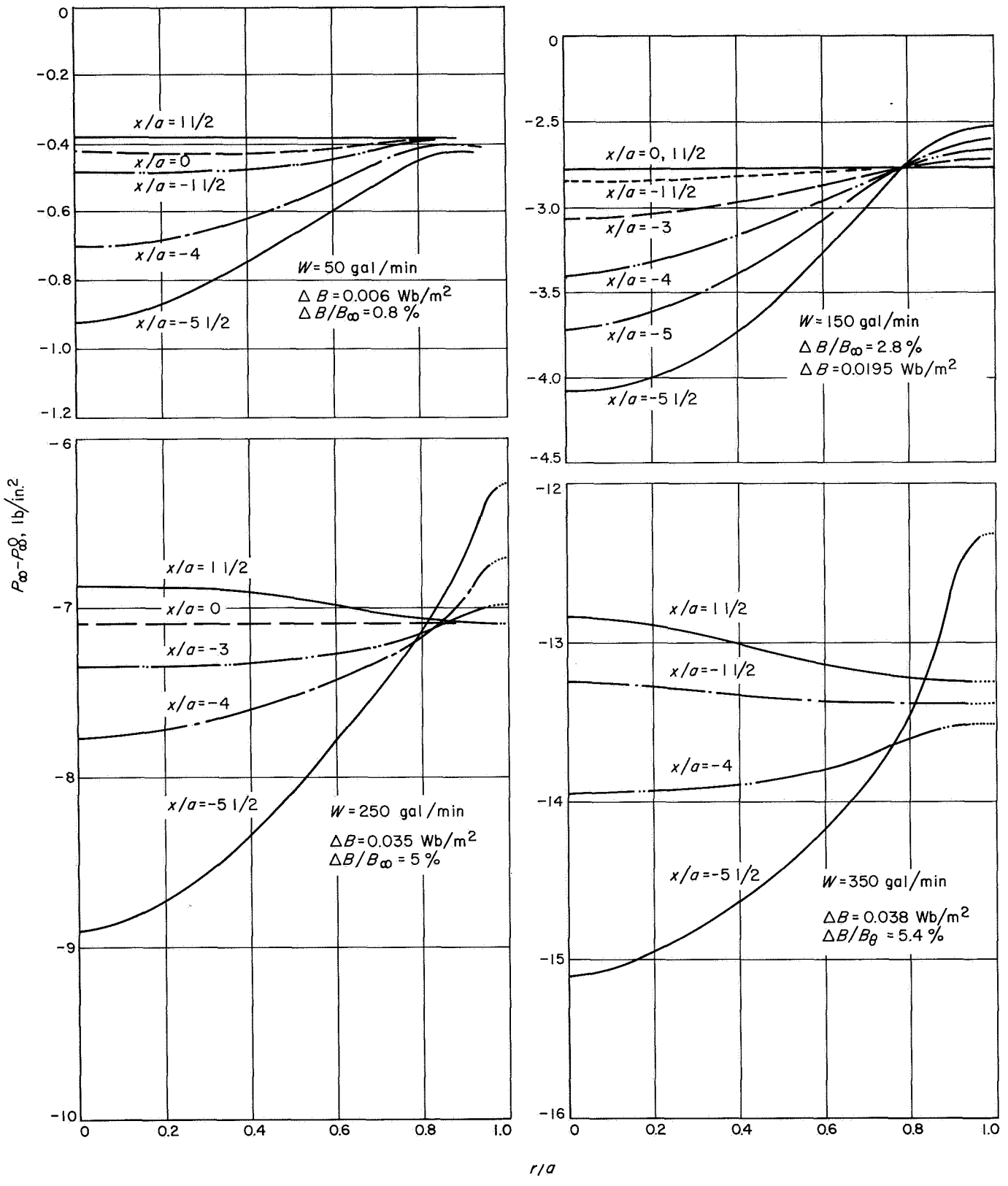

Fig. 6. Radial static pressure profiles at various axial stations and flow rates ($B_\infty = 0.70$ Wb/m^2)

i.e.,

$$-\frac{\partial}{\partial x}\left[P+\frac{1}{2}\rho v_x^2\right]=\rho j_\theta B_r+\nu\frac{\partial^2 v_x}{\partial r^2}+\text{smaller terms,} \tag{6}$$

or

$$-\frac{\partial P^0}{\partial x}=\rho j_\theta B_r+\text{viscous terms} \tag{7}$$

This represents a force balance on a particle, essentially the pressure gradient depending on changes in velocity and on the magnitude of the axial Lorentz force. In the test section, B_r can only be due to some perturbation of the initially axial field and will probably be small. This leads to a suggestion that over the central portion of the flow, at least, axial Lorentz forces will be small. This statement is precise at the center of the tube where both j_θ and B_r are zero from symmetry considerations, and at the walls where $j_\theta = 0$ because v_x and v_r are zero. Therefore, axial pressure gradients on or near the centerline are due to rapid changes in the magnitude of the velocity in that region. Typically, a pressure change of 1400 kg/m² (2 lb/in.²) along the centerline represents a velocity change of 2 m/s at 6 m/s initial velocity. The contribution to the total flow rate of this difference is small so that changes in the rest of the profile do not have to be large in order to compensate for the large increase in central velocity.

This is obvious from a glance at the axial pressure gradients at the wall, which are quite small. Now that we have an order of magnitude for the axial velocity gradient, we can estimate the correctness of our assumption of zero radial acceleration when connecting radial, pressure and magnetic fields as shown in Section IV-B. In a typical case where $\partial v_x/\partial x \approx 20$ m/s/m, then $1/r\ \partial/\partial r\ (rv_r)$ has the same value from continuity. Therefore, between $r = 0$ and $r = a$, v_r changes from zero to 0.05 m/s. The pressure gradient required to cause this acceleration is $\rho/g\ v_r\ \partial v_r/\partial r \approx \rho/g \times 0.05 \times 0.05 \times 10^2 = 25$ kg/m²/m. This is to be compared to the measured radial pressure gradient of about 10^5 kg/m²/m. Acceleration in the radial direction is obviously of negligible effect, and all radial pressure gradients are balanced by radial Lorentz forces only, as assumed in Section IV-B, and below. As a result we can interpret radial pressure variations as the negative of magnetic field variations and calculate the magnetic field and current distributions in the test area. Such a current distribution is shown in Fig. 7, and variations with the parameters are shown in Fig. 8.

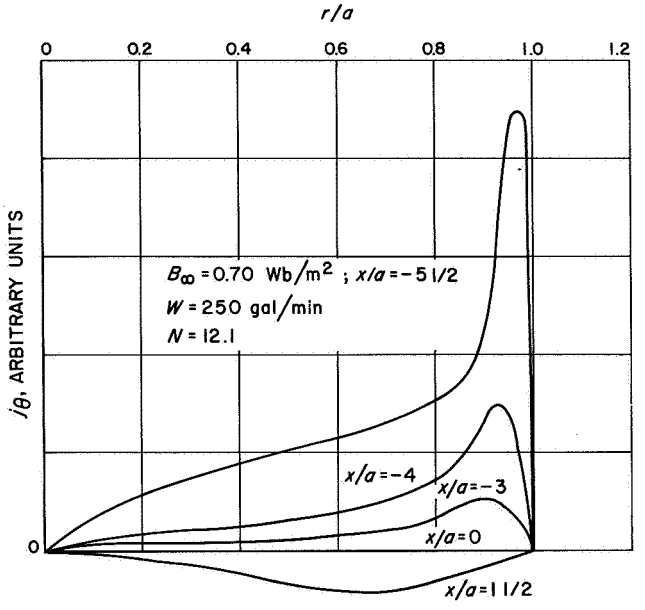

Fig. 7. Distribution of current density j_θ in the test section for $N = 12.1$

From these very straightforward measurements, the following picture emerges. Perturbations in the applied field occur close to the wall in the upper part of the test section. The radial extent of this region grows rapidly as we enter the lower part of the tube in which a large retardation of the fluid close to the wall occurs. Continuity requires that the central velocity increase, thus creating large static pressure gradients in the axial direction. Two possible mechanisms could cause such a slowing of the exit flow close to the wall. Some new type of boundary-layer flow could be invoked. It would obviously have to be very different from ordinary boundary layers, but such an explanation is possible. Another slightly more attractive explanation can be devised which fits in with the limited amount of information already existing on MFD flows. As the flow leaves the magnetic field, several tube diameters below the last measuring station, it is passing through a region with a large applied, radial magnetic field. This fringing field is zero on the centerline and increases monotonically with radius. As the axial flow crosses this field, large azimuthal currents are set up and the flow is retarded the most in regions where the Lorentz force is largest. Most retardation therefore occurs at larger radii where both B_r and v_x are large. Under normal circumstances, one could assume that this retardation is a local affair and would only be felt downstream of the disturbance. Since diffused hydromagnetic or Alfven waves can propagate upstream against the flow, a mechanism exists for the "exit effect" to be felt in the test section itself. This propagation in confined flows is known to have an exponential

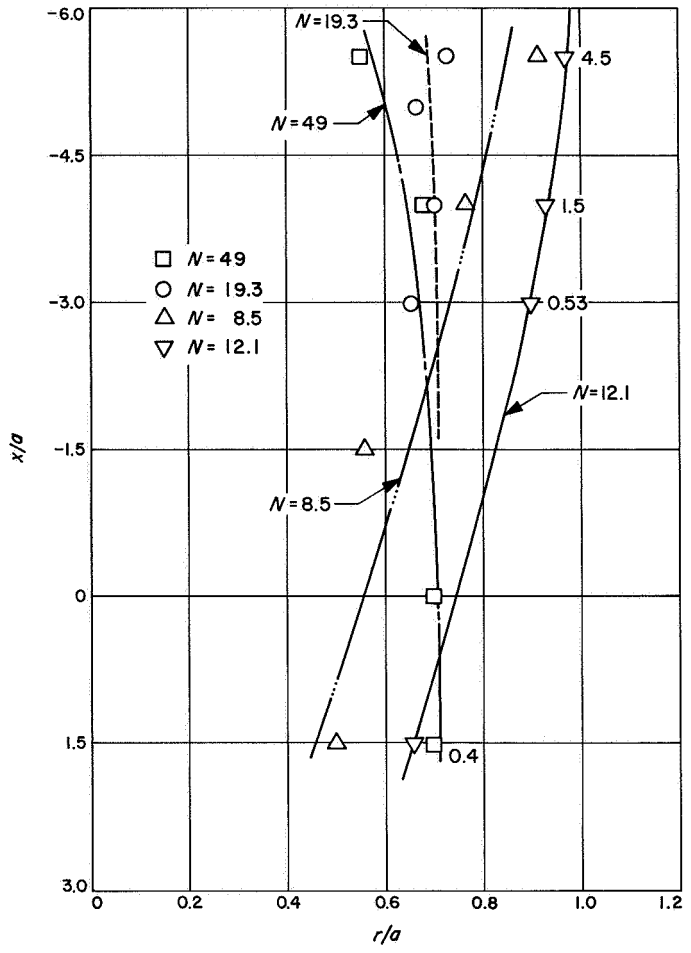

Fig. 8. Variation of current density distribution with N; location of maximum j_θ

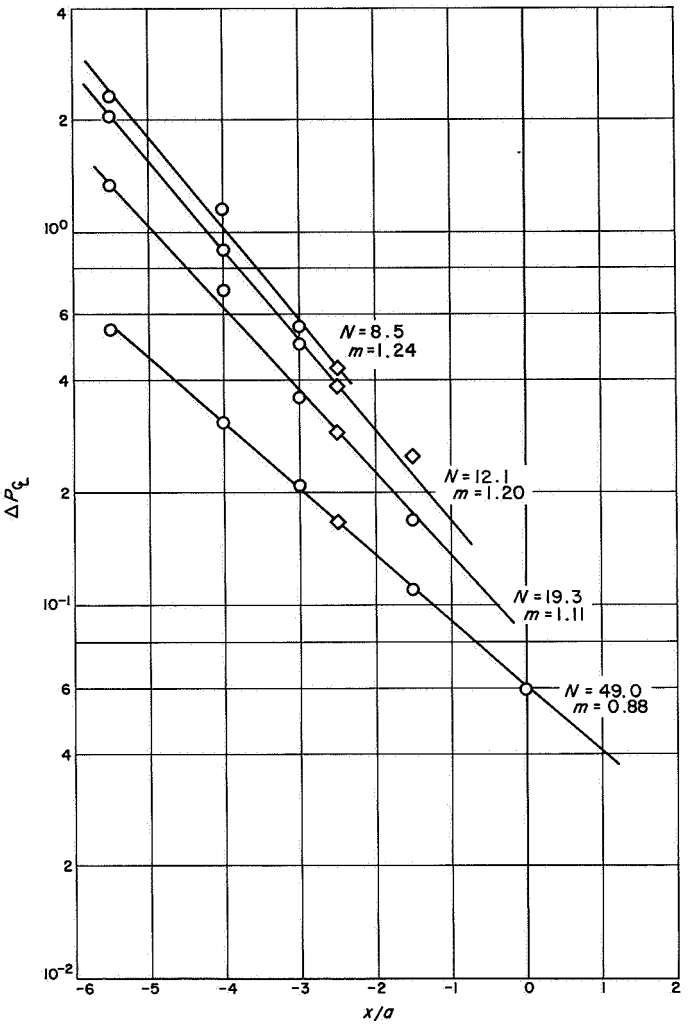

Fig. 9. Variation of static pressure on centerline with axial distance

character (Refs. 6, 7), and our measured profiles indeed show this exponential decay far from the initial disturbance. We can enlarge somewhat on this comparison especially for large N. Suitable replotting of the results shown in Figs. 5 and 6 shows that $\Delta P_{\text{¢}} \approx \exp mx/a$ (Fig. 9)[5], while $b_x \approx x_1^n/a$ (Fig. 10).[6] Only one case, the one with the largest α^2, is considered in Fig. 10 because all of the others contain a substantial effect due to the entry of the fluid into the magnetic field, an effect which completely masks the decay of the exit disturbance. Further comments on the entry phenomenon are given shortly. The value of $n = -2.1$ for this case should be compared with Peyret's value of -2. The exponent m varies with the flow conditions in a way shown in Fig. 11; the results of Peyret's linearized treatment are also indicated. Apparently, the slightly perturbed magnetic field is in substantial agreement, while the greatly perturbed velocity and pressure fields are not. Nevertheless, the suggestion that it is a propagation of exit disturbances upstream which is causing the observed changes is verified, because this is the only mechanism allowed by the inviscid, linear theory.

At a given field strength, the nature of the exit disturbance changes as the flow velocity is changed. In particular, as Alfven number unity is traversed from the sub-Alfvenic side, the decay changes from an exponential form to a form more characteristic of regular pipe flow. Other observations also reinforce this view. At high magnetic fields the exit centerline pressure gradients are almost

[5] Where $\Delta P_{\text{¢}}$ is the difference in pressure between entry into the measuring section and the point in question, measured along the center line.

[6] x_1 is the distance measured upstream from the location where the applied magnetic field begins to fringe.

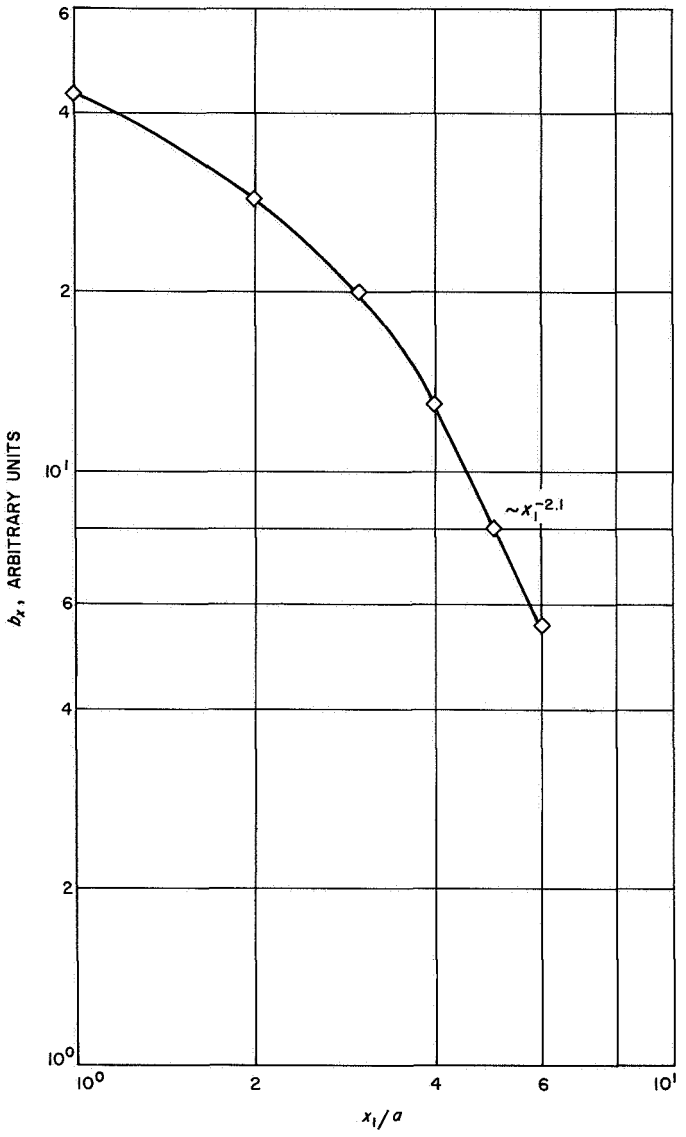

Fig. 10. Variation in centerline magnetic field perturbation with axial distance from exit of magnet

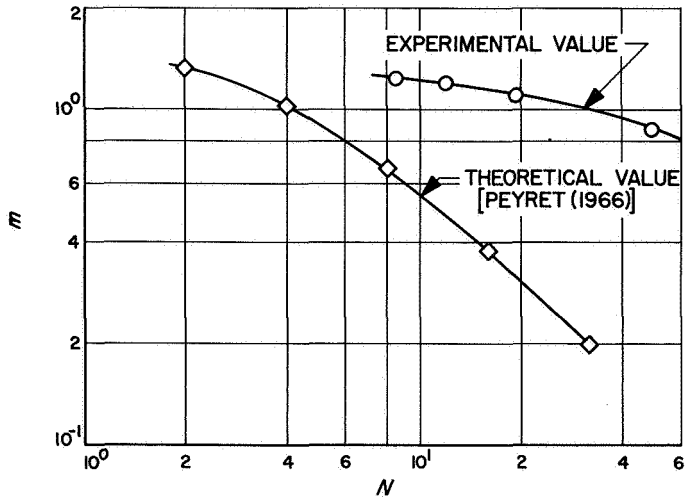

Fig. 11. Variation of exponent *m* with *N*

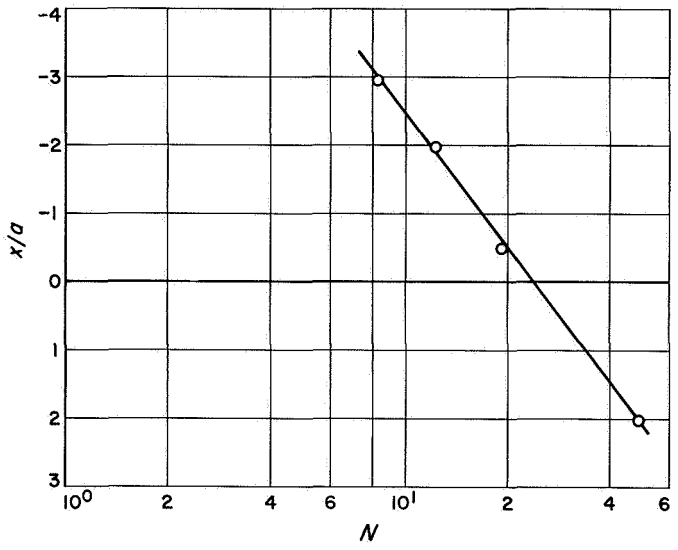

Fig. 12. Location of the cross-section at which the current density changes sign

independent of flow rate from 100 to 350 gal/min. An explanation based on boundary-layer considerations is hard to construct, but in terms of the exit phenomena it becomes rather more reasonable. At constant field strength the intensity of the exit effect, where it is initially formed, depends on the flow velocity. The intensity with which it can propagate upstream against the oncoming stream depends inversely on the stream velocity. Apparently the result of these two conflicting effects is to give a net result which is changed very little over a wide range of velocities. As an Alfven number of unity is approached, there is no doubt that this is no longer true and a more complicated picture should result.

Radial variations in static pressure provide further insight into the nature of these flows when interpreted more completely in ranges where the exit effect is not dominant. Certain anomalies in our previous discussion result which have to be resolved by introducing an "entry effect." There is a region where the current density changes sign. In fact, in most cases there is actually a region where there are no currents across a particular section. The location of this section changes with the parameters as shown in Fig. 12. Since the exit effect can only give *clockwise* currents (designated *positive* for convenience), then the negative or anticlockwise currents must come from the interaction upstream of the test section, i.e., from a vestigial entry

effect that was not completely eliminated by the nozzle-shaping procedure described in Section III-A. Interestingly, at large N the exit effect propagating upstream dominates the entry effect being both propagated and convected downstream.

From this discussion, it is also clear that pressure measurements made only at wall pressure taps do not give a correct representation of the flow in the pipe and should be interpreted with extreme caution when they are the only diagnostic measurement made.

B. Deductions from Measurements of Total Pressure

As can be seen from Eq. (6), two effects can change the total pressure in the tunnel as measured by a pitot tube: axial magnetic forces, caused by the perturbation of the originally axial field, and viscous shear stresses mainly associated with curvature of the v_x velocity profile. This formulation is slightly misleading since it suggests a possible increase of P^0 in the downstream direction. To see that this cannot in fact be so, we observe that, as long as no external electric field is applied, the motion of a particle across a field line must always result in a force which reduces the total pressure in the direction of motion. In slightly more mathematical terms, using Tamada (Ref. 8),

$$P^0 + \frac{\alpha^2}{R_m}\int_{-\infty}^{s}\frac{1}{q}\,j^2 ds = \text{constant along a streamline}$$

$$= P^0(-\infty)$$

where ds is a line element along a stream tube.[7] The second term is always positive and increases with s, hence P^0 is always decreasing along a streamline, by an amount equal to the integrated Joule dissipation to the point in question. On the axis of symmetry, only viscous effects can cause any variation of the total pressure. Any change in total pressure along the centerline is thus representative of curvature of the velocity profile and means that vorticity exists everywhere downstream of the first location of a substantial centerline total-pressure decrease. This statement, in turn, assumes that the dissipation, or viscous shear stresses, caused by probe interactions are smaller by at least an order of magnitude. The same arguments hold for the flow along the wall. There the azimuthal current falls to zero and the Lorentz force does the same even though B_r is not necessarily zero. Between, there is no reason to ignore the Lorentz force. We can in fact estimate its value from other measurements already described, and show its importance.

The term j_θ comes from the measurements of static pressure:

$$j_\theta \approx \mu\frac{\partial B_x}{\partial r} = -\frac{\mu^2}{B_{x_0}}\frac{\partial P}{\partial r}, \text{ since } P + \frac{B_x^2}{2\mu} = f(x)$$

where $f(x)$ is a measured function of x; and

$$B_x \equiv B_{x_0} + b_x, \text{ with } b_x \ll B_{x_0}$$

The term B_r comes from estimating $\partial B_x/\partial x$, setting this equal to $-1/r[\partial(rB_r)/\partial r]$ (since div $\mathbf{B} = 0$), and integrating across the radius, i.e.,

$$B_r = -\frac{1}{r}\int_0^r r\frac{\partial B_x}{\partial x}\,dr$$

$$\equiv \frac{\mu}{B_{x_0}\,r}\int_0^r r\left[\frac{\partial P}{\partial x} - \frac{\partial f}{\partial x}\right]dr$$

For small r, $\partial P/\partial x$ is almost constant; therefore,

$$B_r \approx \frac{\mu r}{2B_{x_0}}\left[\frac{\partial P}{\partial x} - \frac{\partial f}{\partial x}\right]$$

whence

$$\frac{1}{\rho}\frac{\partial P^0}{\partial x} \approx \frac{\mu^3 r}{2B_{x_0}^2}\frac{\partial P}{\partial r}\left[\frac{\partial P}{\partial x} - \frac{\partial f}{\partial x}\right]$$

From such estimates, the greatest effects occur at $r/a \sim 0.5$, i.e., away from wall, viscous, boundary-layer effects, but where j_θ is close to a maximum. These give values of $\partial P^0/\partial x$ of the same magnitude as those measured directly. These results also confirm that entry effects cannot be completely ignored and that Joule dissipation is taking place ahead of the upstream probe station. When we wonder about the effect this has on the performance of the device as a wind tunnel, we find that under the worst circumstances the loss in P^0, i.e., (ΔP^0), compared to P^0_∞ is 1% at the location of the test body radius and 4% at twice that radius. We are confident that the test body is in a region where the approach stream has essentially a constant distribution of total pressure (Fig. 13).

[7] $\frac{1}{q}$ represents the variation in cross-sectional area of the stream tube.

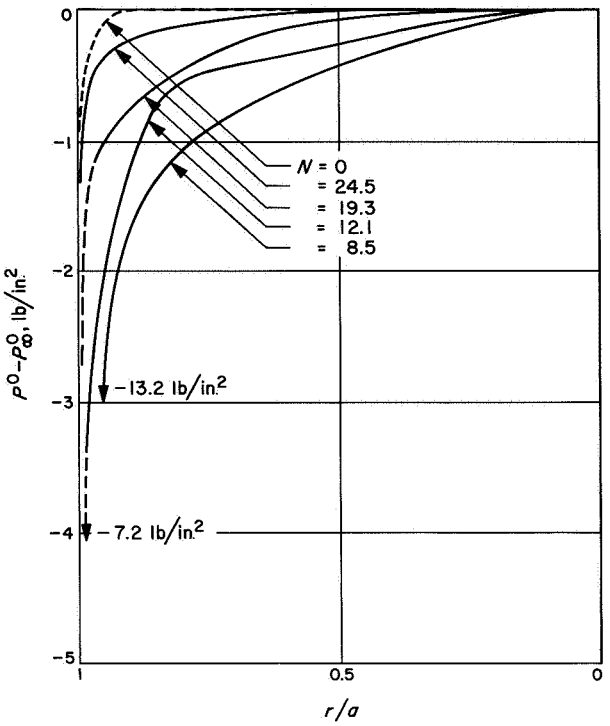

Fig. 13. Variation of total pressure in test section (x = 0) at fixed magnetic field strength and variable flow rate

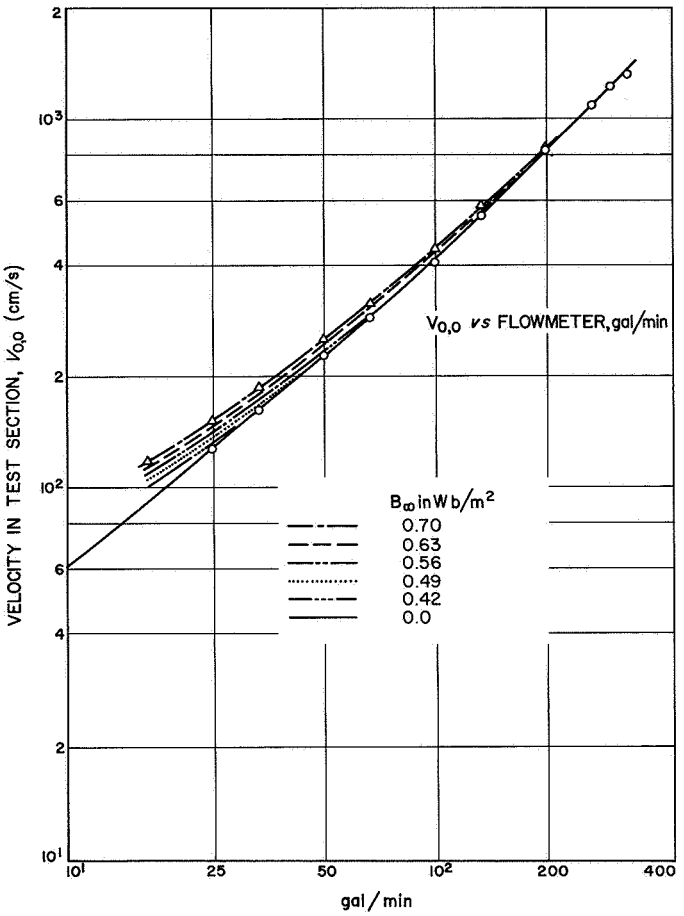

Fig. 14. Velocity calibration curves

C. Velocity Measurements

By combining the total and static-pressure measurements of the previous section, or by measuring $P^0 - P$ directly using a specially constructed pitot-static probe, traverses of velocity can be presented. One correction has been applied to all of the velocity data presented here. The existence of axial gradients in the static pressure means that the static hole and the total hole are in regions of different velocity or alternatively different static pressure. Actual measurements of this pressure difference have been made and applied to the measurements of velocity in order to remove this confusing feature from the results.

The accuracy and repeatability with which we can make one traverse to measure the important quantities across and along the tunnel are less than the accuracy to within which we need to know them for aerodynamic testing. This is particularly true of the dynamic pressure Q of the approach flow at the testing location at low flow rates, i.e., less than a nominal 50 gal/min. Therefore, many repeated measurements of Q were taken at the test location under all possible circumstances of flow rate and field strength, and the corresponding velocity calibrations are shown in Fig. 14. A cross plot vs field strength at constant flow rate shows the remarkable feature that there is no effect until a certain critical field is reached, and then the central Q departs from the no-field case at a rate approximately proportional to $B_\infty^{1/2}$.

Representative velocity profiles are shown in Fig. 15. The statements made in Sections V-A and B are verified, with accelerations occurring on the centerline, and a distinct hump in the profiles appearing as the magnetic field is increased. Again, in the test section the vorticity is small, being of the order of 1% of U_∞/a at the location of the test body radius.

D. Flow Characteristics with Modified Magnetic Field

In order to crudely check the effect of entry into a magnetic field with no upstream flow shaping, i.e., to estimate the effectiveness of our nozzle design, the following tests were performed. The solenoid is made up of two halves electrically connected in parallel. By disconnecting either of the halves, measurements could be made in the

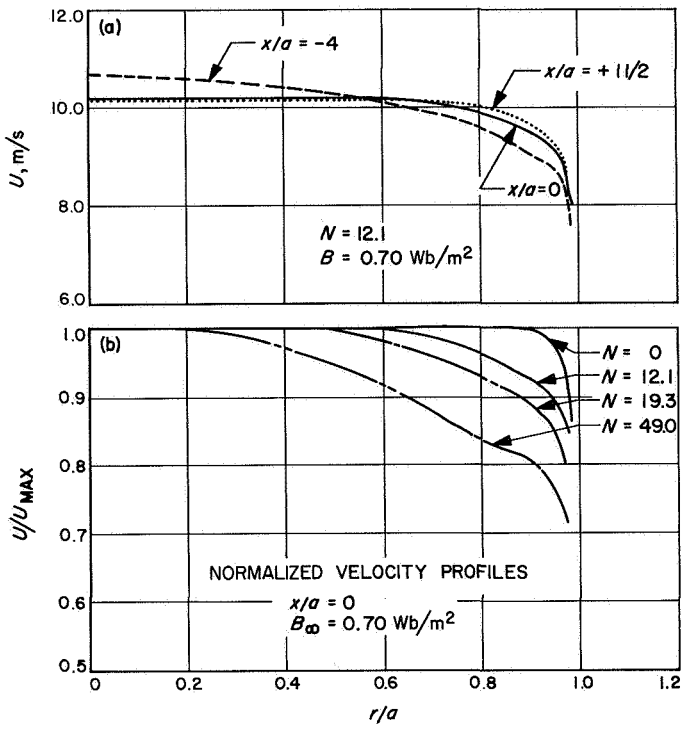

Fig. 15. Velocity profiles: (a) velocity profiles at various axial locations for $N=12.1$; (b) normalized velocity profiles for $B_\infty=0.70$ Wb/m², various N at the center of the magnet, $x/a=0$

magnetic field produced by the other half alone. Of particular interest was the flow through the lower half of the magnet as sketched in Fig. 3(a). Such a configuration was found to introduce enormous changes in the flow field and magnetic field as indicated, for example, by the pressure profiles of Fig. 16, which are to be compared to Fig. 5. Apparently our nozzle-shaping procedure was necessary. Also desirable, but difficult from an engineering point of view, would have been a shaping of the exit flow.

VI. Conclusions

The flow characteristics of the JPL liquid sodium tunnel have been described and the majority of the perturbations from uniform flow blamed on the propagation of exit disturbances into the test section.

It is concluded that the tunnel is suitable for aerodynamic testing except under the most extreme conditions of magnetic field strength and flow velocity.

Even under circumstances where the flow seems to be quite perturbed, correct answers are obtained if all parameters are based on local conditions. This statement is verified by results presented in the Appendix, where it is found that the pressure distribution around a sphere is independent of the location of the body in the test section as long as *local* flow properties are used.

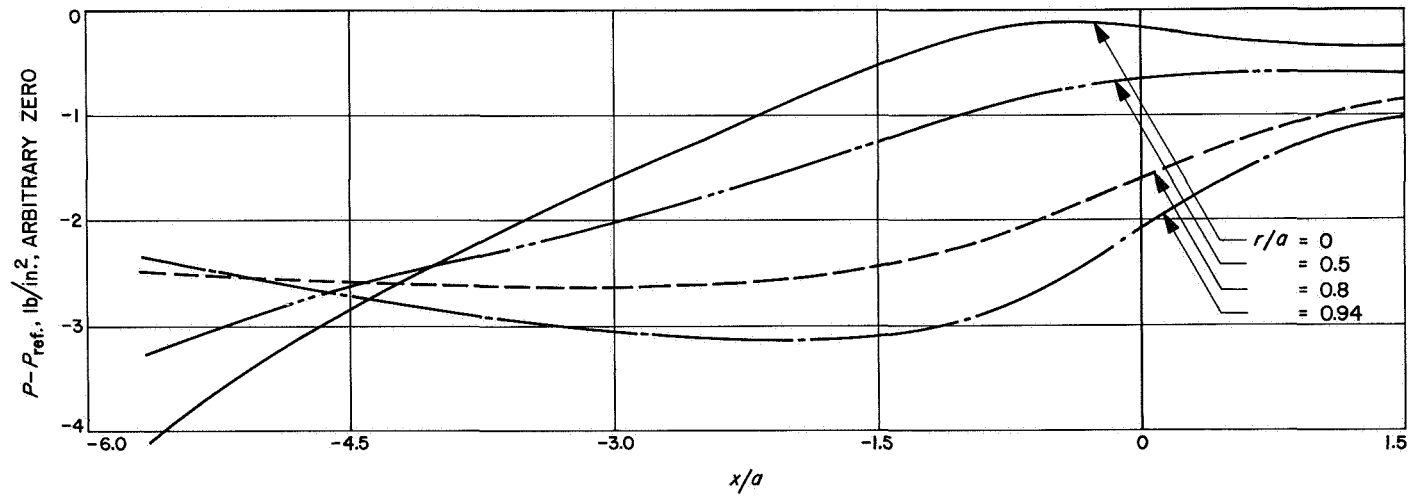

Fig. 16. Longitudinal static pressure profile in magnet with no shaping of the inlet flow $B_\infty=0.70$ Wb/m², $N=12.1$

Appendix
Pressure Distribution Measurements

Presented herein is independent evidence on the usefulness of the sodium tunnel as a device for accurate determination of MFD flows. Included are measurements around a sphere placed at various axial locations within the test section. The evidence is a natural extension of the work described by Maxworthy (Ref. 3). This was not described in that article because it was felt that it would unnecessarily complicate and perhaps obscure the simple results presented therein. Because the results to be presented in this Appendix are mainly concerned with the effects the exit perturbations might have on aerodynamic flows in the tunnel, it is just as natural to place the results in this report which is primarily concerned with the usefulness of the tunnel as an aerodynamic testing facility.

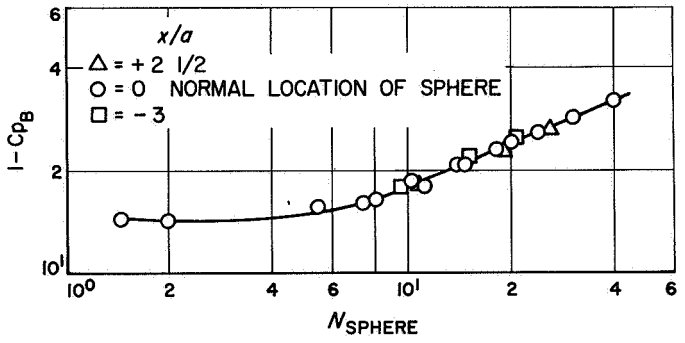

Fig. A-1. $1 - C_{p_B}$ vs N sphere, for test sphere located at several axial positions within tunnel

The sphere described by Maxworthy (Ref. 3), and used to measure the pressure distribution as a function of angle around a circle of longitude, was operated at 3 axial locations within the test section. Using the tunnel calibration curves, and the known variation of axial velocity along the tunnel, local values of velocity and magnetic field were calculated. These local values were then used to reduce the measured pressure distribution. Figure A-1 shows this reduction by plotting the base pressure coefficient C_{p_B},* as a function of the local value of the interaction parameter. As to the accuracy of the experiment, it is not possible to tell the difference between results taken at the different locations, and the gross features at least do not depend on the perturbed flow created by the exit disturbance. It suggests that the distortion of the wake structure, especially downstream, is not critically important in determining the pressures on the sphere.

*$C_{p_B} = \dfrac{P_B - P_\infty}{1/2\,\rho\,U^2}$, where P_B is the base pressure, and U the local velocity.

References

1. Yonas, G., "Aligned Fields, Magneto-Fluid-Dynamic Flows Past Bodies," Ph.D. Dissertation, California Institute of Technology, Pasadena, Calif., 1966.
2. Yonas, G., "Aligned Fields, Magneto-Fluid-Dynamic Drag Measurements With Large Interaction Parameters," *J. Fluid Mech.* (in publication).
3. Maxworthy, T., "Experimental Studies in Magneto-Fluid-Dynamics: Pressure Distribution Measurements Around a Sphere," *J. Fluid Mech.* (in publication).
4. *Liquid Metals Handbook*, Atomic Energy Commission, Dept. of the Navy, Washington, D.C., 1952; Na-K Supplement, 1955.
5. Schubauer, G. B., and Spangenburg, W. G., *Effect of Screens in Wide-Angle Diffusers,* TN 1610, National Advisory Committee for Aeronautics, Washington, D.C., 1948.

References (contd)

6. Ahlstrom, H., "Experiments on the Upstream Wake in Magneto-Fluid Dynamics," *J. Fluid Mech.*, Vol. 15, 1963.

7. Peyret, R., *Sub-Alfvenic Flow in a Duct With a Nonuniform Magnetic Field*, Technical Report 32-871, Jet Propulsion Laboratory, Pasadena, Calif., April 15, 1966.

8. Tamada, K., "Flow of a Slightly Conducting Fluid Past a Circular Cylinder With Strong Aligned Field," *Phys. Fluids*, Vol. 5, pp. 817–823, 1962.